Journal of Fluorescence, Vol. 14, No. 4, July 2004 (©2004)

Using Solution-Phase Nanoparticles, Surface-Confined Nanoparticle Arrays and Single Nanoparticles as Biological Sensing Platforms

Amanda J. Haes,[1] Douglas A. Stuart,[1] Shuming Nie,[2] and Richard P. Van Duyne[1,3]

Received November 1, 2003; revised January 29, 2004; accepted January 29, 2004

The intense colors of noble metal nanoparticles have inspired artists and fascinated scientists for hundreds of years. In this review, we describe three sensing platforms based on the tunability of the localized surface plasmon resonance (LSPR) of gold and silver nanoparticles. Specifically, the color associated with solution-phase nanoparticles, surface-confined nanoparticle arrays, and single nanoparticles will be shown to be tunable and useful as platforms for biological sensing.

KEY WORDS: Nanoparticles; localized surface plasmon resonance; biosensor; streptavidin; immunoassay.

INTRODUCTION

Recent years have seen an increase in the implementation of fluorescence for biological assays, detection, labeling, and sensing. While fluorescence based biological assays have become standard in industry and academia, nanoparticle based techniques provide several alternatives to these conventional methods, including: nanoparticle barcode labels [1], resonant Rayleigh scattering [2,3], nanoparticle aggregation [4], local refractive index changes [5,6], and charge transfer interactions [5,7].

The intense scattering and absorption of light from noble metal nanoparticles is the source of the beautiful colors in stained glass windows and has attracted the interest of scientists for generations (Fig. 1). Although scientists have learned that the characteristic hues of these noble metal nanoparticle suspensions arise from their strong interaction with light, the advent of the field of nanoparticle optics allowed for a deep understanding of the relationship between material properties such as composition, size, shape, and local dielectric environment and the observed color of a metal suspension. An understanding of the optical properties of noble metal nanoparticles holds both fundamental and practical significance. Fundamentally, it is important to systematically explore the nanoscale structural and local environmental characteristics that cause optical property variation as well as provide access to regimes of predictable behavior. Practically, the tunable optical properties of nanostructures can be applied as materials for surface-enhanced spectroscopy [8–12], optical filters [13,14], plasmonic devices [15–17], and sensors [6,7,18–24].

Noble metal nanoparticles exhibit a strong UV-visible absorption band that is not present in the spectrum of the bulk metal. This absorption band results when the incident photon frequency is resonant with the collective excitation of the conduction electrons and is known as the localized surface plasmon resonance (LSPR). LSPR excitation results in wavelength selective absorption with extremely large molar extinction coefficients $\sim 3 \times 10^{11}$ M^{-1} cm^{-1} [25–27], resonant Rayleigh scattering [28,29] with an efficiency equivalent to that of 10^6 fluorophors [3,30,31], and the enhanced local electromagnetic fields near the surface of the nanoparticle which are responsible

[1] Department of Chemistry, Northwestern University, 2145 Sheridan Road, Evanston, Illinois 60208-3113.
[2] Departments of Biomedical Engineering and Chemistry, Emory University and Georgia Institute of Technology, Pierce Drive Suite 2001, Atlanta, Georgia.
[3] To whom correspondence should be addressed. E-mail: vanduyne@chem.northwestern.edu.

1053-0509/04/0700-0355/0

Fig. 1. The rose window at the Notre Dame Cathedral, Paris, France, 2002.

for the intense signals observed in all surface-enhanced spectroscopies [10].

The simplest theoretical model for the optical properties of nanoparticles is the Mie theory result for the extinction of a metallic sphere in the long wavelength, electrostatic dipole limit. In the following equation: [32]

$$E(\lambda) = \frac{24\pi N_A a^3 \varepsilon_m^{3/2}}{\lambda \cdot \ln(10)} \left[\frac{\varepsilon_i(\lambda)}{(\varepsilon_r(\lambda) + 2\varepsilon_m)^2 + \varepsilon_i^2(\lambda)} \right] \quad (1)$$

$E(\lambda)$ is the extinction (viz., sum of absorption and scattering), N_A is the areal density of nanoparticles, "a" is the radius of the metallic nanosphere, ε_m is the dielectric constant of the medium surrounding the metallic nanosphere (assumed to be a positive, real number and wavelength independent), λ is the wavelength of the absorbing radiation, ε_i is the imaginary portion of the metallic nanosphere's dielectric function (wavelength dependent), and ε_r is the real portion of the metallic nanosphere's dielectric function (wavelength dependent). Even in this simplified model, it is abundantly clear that the intensity of the LSPR spectrum of an isolated metallic nanosphere embedded in an external dielectric medium will depend on the nanoparticle radius "a." Similarly, the wavelength of the maximum extinction, λ_{max}, will depend on the nanoparticle material ($\varepsilon_i(\lambda)$ and $\varepsilon_r(\lambda)$), and the nanoenvironment's dielectric constant (ε_m). Furthermore, when the nanoparticles are not spherical, as is always the case in real samples, the extinction spectrum also depends on the nanoparticle's in-plane diameter, out-of-plane height, and shape. The dependence of the extinction spectrum on these nanoparticle structural parameters has been described for ellipsoidal nanoparticle geometries [26]. In this case the denominator of the resonance term in equation 1 is replaced with:

$$(\varepsilon_r(\lambda) + \chi\varepsilon_m)^2 \quad (2)$$

where χ is a term that describes the nanoparticle aspect ratio. The values for χ increase from 2 (for a sphere) up to, and beyond, values of 17 for a 5:1 aspect ratio nanoparticle. In addition, many of the samples considered in this work contain an ensemble of nanoparticles that are supported on a substrate. Thus, the spectral position of the LSPR will also depend on interparticle spacing and substrate dielectric constant [26,27,33–38].

There are several synthetic routes to develop nanoparticles with tunable plasmonic properties. The most common approach is through the reduction of a metal salt in solution to form noble metal colloidal suspension. Typically, size control is achieved by varying the concentration of the starting reagents and the strength of the reductant. In Fig. 2, a series of gold and silver spherical nanoparticles with varying diameters were synthesized

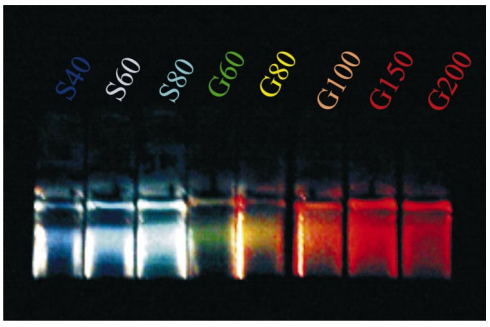

Fig. 2. Various sizes of spherical silver and gold colloids illuminated with a white light beam, showing the effect of particle composition and size on the resonant scattering wavelength. Silver colloids prepared with 40, 60, and 80 nm (S40, S60, and S80) exhibit significantly shorter wavelength scattering than the gold colloids of 60, 80, 100, 150 and 200 nm diameters (G60, G80, G100, G150 and G200). Both materials show a trend towards longer wavelength scattering as the size of the nanoparticle increases.

using this method. As clearly demonstrated in the figure, both material size and composition affect the color of the scattering of the solution. For example, an 80 nm silver nanoparticle selectively scatters blue light and the equivalent gold nanoparticle scatters yellow light; 60 nm and 200 nm gold nanoparticles scatter green and red, respectively.

An alternative approach for producing more precisely controlled nanoparticles is through a technique known as nanosphere lithography (NSL) (Fig. 3A). NSL is a powerful fabrication technique that inexpensively produces nanoparticle arrays with controlled shape, size, and interparticle spacing [39]. The need for monodisperse, reproducible, and materials general nanoparticles has driven the development and refinement of the most basic NSL architecture as well as many new nanostructure derivatives. Every NSL structure begins with the self-assembly of size-monodisperse nanospheres of diameter D to form a two-dimensional colloidal crystal deposition mask. Methods for deposition of a nanosphere solution onto the desired substrate include spin coating [39], drop coating [40], and thermoelectrically-cooled angle coating [41]. All of these deposition methods require that the nanospheres be able to freely diffuse across the substrate seeking their lowest energy configuration. This is often achieved by chemically modifying the nanosphere surface with a negatively charged functional group such as carboxylate or sulfate that is electrostatically repelled by the negatively charged surface of a substrate such as mica or glass. As the solvent (water) evaporates, capillary forces draw the nanospheres together, and the nanospheres crystallize in a hexagonally close-packed pattern on the substrate. As in all naturally

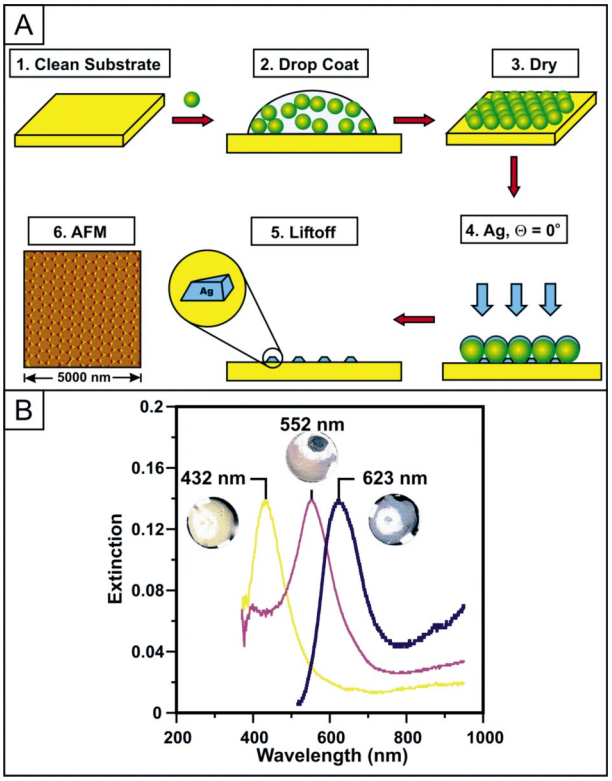

Fig. 3. (A) Ag nanoparticles were fabricated using NSL. Six steps are required for the synthesis of the nanoparticles: (1) glass or mica substrates are cleaned, (2) monodisperse polystyrene nanospheres are drop-coated onto the substrate, (3) a single layer of hexagonally close packed nanospheres dries creating a nanosphere mask, (4) Ag metal is vapor deposited onto the sample, (5) the nanosphere mask is removed via sonication in ethanol, and (6) the Ag nanoparticle sample is prepared for sensing experiments. (B) Extinction spectra and photographs of Ag nanoparticle array samples synthesized using NSL. The LSPR of Ag nanoparticles blue-shifts from 623 to 552 to 432 nm as the shape of the nanoparticles are thermally annealed under vacuum. The peak at 623 nm arises from triangular nanoparticles. The peak at 552 nm arises from triangular nanoparticles with blunted tips. The peak at 432 nm arises from hemispherical nanoparticles. All samples were synthesized using a 400 nm nanosphere mask.

occurring crystals, nanosphere masks include a variety of defects that arise as a result of nanosphere polydispersity, site randomness, point defects (vacancies), line defects (slip dislocations), and polycrystalline domains. Typical defect-free domain sizes are in the 10–100 μm range. Following self-assembly of the nanosphere mask, a metal or other material is then deposited by thermal evaporation, electron beam deposition, or pulsed laser deposition from a collimated source normal to the substrate through the nanosphere mask to a controlled mass thickness, d_{m}. After metal deposition, the nanosphere mask is removed, typically by sonicating the entire sample in a

solvent, leaving behind the material deposited through the nanosphere mask and onto the substrate [39].

Just as in solution phase syntheses, NSL can be used to synthesize tunable optical properties of noble metal nanoparticles (Fig. 3B). In this figure, the optical properties of surface-confined silver nanoparticles are varied by changing their shape through thermal annealing. The inset photographs show representative samples at three stages of annealing. As the nanoparticles change shape from triangles to spheres, the position of the extinction maximum (and therefore color) shifts from 623 to 432 nm. Tunability of the LSPR from the UV to the near infrared region of the spectrum can also be achieved by varying the in-plane width and out-of-plane height of the nanoparticles [25].

BIOSENSING WITH NANOPARTICLES

The development of biosensors for the diagnosis and monitoring of diseases, drug discovery, proteomics, and the environmental detection of biological agents is an extremely significant problem [42]. Fundamentally, a biosensor is derived from the coupling of a ligand-receptor binding reaction [43] to a signal transducer. Much biosensor research has been devoted to the evaluation of the relative merits of various signal transduction methods including optical [44,45], radioactive [46,47], electrochemical [48,49], piezoelectric [50,51], magnetic [52,53], micromechanical [54,55], and mass spectrometric [56,57]. Although each of these methods has its individual strengths and weaknesses, a strong case has been made that sensors based on optical transduction methods are advantageous for numerous applications [58]. Recently, several research groups have begun to explore alternative strategies for the development of optical biosensors [4,5,33,59–74] and chemosensors [5,75–80] based on the extraordinary optical properties of noble metal nanoparticles.

Solution phase nanoparticle based sensing is a simple, yet powerful detection modality. Because many molecules of interest, particularly biological molecules, are in the aqueous phase, it is desirable to have a sensitive and specific detection system that is homogenous with the phase of the target molecule, thereby decreasing the need for extended sample preparation. Aggregation based detection has become a mainstay in the clinical community since the development of the Latex Agglutination Test, or LAT, in 1956 [81]. In the LAT and similar tests, biomolecularly specific antibodies are conjugated to latex microspheres which, when mixed with a solution (e.g. blood or urine) containing the target antigen, cause the latex spheres to form visible aggregates. While LATs are effective and quite rapid (15 min to 1 hr), they are inherently insensitive, relying on high concentrations of analytes and on the human eye as a detector.

In contrast, for solution-phase LSPR based sensing, signal transduction depends on the sensitivity of the surface plasmon to interparticle coupling. When multiple particles in solution that support a localized surface plasmon are in close proximity (i.e. interparticle spacings less than the nanoparticle diameter), they are able to interact electromagnetically through a dipole coupling mechanism. This broadens and red shifts the LSPR, and small clusters of particles posses LSPR properties similar to those of a larger single particle. Two methods of detection readily lend themselves to monitoring these changes in the position of the localized surface plasmon resonance: UV-visible (UV-vis) extinction (absorption plus scattering) and resonant Rayleigh scattering spectroscopy.

Recently, several papers have been published on a gold nanoparticle based UV-vis technique for the detection of DNA. This colorimetric detection method is based on the change in absorbance spectra (i.e. color) as particles are brought together by the hybridization of complementary DNA strands [4,18,65,73,74,82,83]. The limits of detection (LOD) reported are in the range of tens of femtomoles of target oligonucleotide. These nanoparticle aggregation assays represent a 100-fold increase in sensitivity over conventional fluorescence-based assays [82].

SOLUTION-PHASE NANOPARTICLE SENSTING

Sensing based on resonant Raleigh scattering detection is a potentially more powerful, yet less well published, method than the colorimetric technique mentioned above [84]. Figure 4 demonstrates a simple sensing experiment. A rapid test for biomolecular reactivity was designed that relies on the change in optimal scattering wavelength induced by interparticle coupling as the signal transduction method. Four mL of anti-human IgG/60 nm gold particles and 4 mL of human IgG/60 nm gold particles were mixed in a glass vial under stirring. A beam of white light was used to illuminate the sample vial, and the colorful scattered light was recorded with a digital camera. The complementary proteins bind to each other causing the gold nanoparticles to be brought into closer proximity. As a result, the gold particles were able to electromagnetically couple, resulting in a pronounced red shift of the LSPR. As seen in Fig. 4, the color of the scattered light changed noticeably from (A) green to (B) yellow to (C) orange in the space of about 15 min, indicating nanoparticle aggregation, which is indicative of a positive binding event. The disadvantages of this type of experiment is

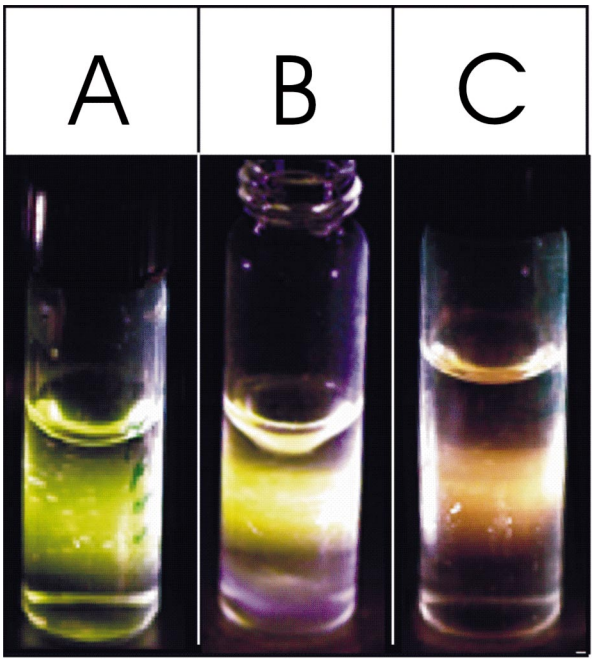

Fig. 4. Time lapse photos of the rapid colorimetric test. (A) 60 nm gold conjugates. (B) Stirring 1:1 solution of IgG/gold conjugates and anti-human IgG/gold conjugates after approximately 3 minutes of stirring. (C) The same solution as (B), approximately 10 minutes later. Note the readily observed change in color from green to orange. This color change is caused by interparticle coupling.

that the aggregation of the particles, necessary to induce interparticle coupling and generate a signal, is often irreversible, difficult to quantitate, and can lead to sufficient aggregation of the nanoparticles that they settle out of solution.

A possible method to circumvent the issue of irreversible complex formation is to synthesize nanoparticles bound to substrates. Using this method, we have demonstrated that nanoscale chemosensing and biosensing could be realized through shifts in the localized surface plasmon resonance (LSPR) extinction maximum (λ_{max}) of triangular silver nanoparticles [5,6,20,24]. Instead of being caused by the electromagnetic coupling of the nanoparticles, these wavelength shifts are caused by adsorbate-induced local refractive index changes in competition with charge-transfer interactions at the surfaces of nanoparticles.

STREPTAVIDIN SENSING ON NANOPARTICLE ARRAYS USING LSPR SPECTROSCOPY

The well-studied biotin-streptavidin system with its extremely high binding affinity ($K_a \sim 10^{13}$ M^{-1}) [85] is chosen to illustrate the attributes of these LSPR based nanoscale affinity biosensors. The biotin-streptavidin system has been studied in great detail by flat surface, propagation surface plasmon resonance (SPR) spectroscopy [86,87] and serves as an excellent model system for the LSPR nanosensor [6,88]. Streptavidin, a tetrameric protein, can bind up to four biotinylated molecules (i.e. antibodies, inhibitors, nucleic acids, etc.) with minimal impact on its biological activity [88] and, therefore, will provide a ready pathway for extending the analyte accessibility of the LSPR nanobiosensor.

NSL was used to create surface-confined triangular Ag nanoparticles supported on a glass substrate (Fig. 3A). The Ag nanotriangles have in-plane widths of ∼100 nm and out-of-plane heights of ∼51 nm as determined by AFM. To prepare the LSPR nanosensor for biosensing events, the Ag nanotriangles are first functionalized with a self-assembled monolayer (SAM) composed of 3:1 1-octancethiol:11-mercaptoundecanic acid (1-OT:11-MUA) resulting in a surface coverage corresponding to 0.1 monolayer of carboxylate binding sites. Since the maximum number of alkanethiol molecules per nanoparticle is 60,000, this is equivalent to ∼6000 carboxylate binding sites per nanoparticle. Next, biotin was covalently attached to the carboxylate groups using a zero-length coupling reagent. The number of resulting biotin sites will be determined by the yield of this coupling reaction. Since this is likely to be ∼1–5% efficient one expects there to be only 60–300 biotin sites per nanoparticle at maximum coverages.

Before surface functionalization, the Ag nanoparticles were exposed to solvent and N_2 as described above. In this study, the λ_{max} of the Ag nanoparticles were monitored during each surface functionalization step (Fig. 5A). First, the LSPR λ_{max} of the bare Ag nanoparticles was measured to be 561.4 nm (Fig. 5A-1). To ensure a well-ordered SAM on the Ag nanoparticles, the sample was incubated in the thiol solution for 24 h. After careful rinsing and thorough drying with N_2 gas, the LSPR λ_{max} after modification with the mixed SAM (Fig. 5A-2) was measured to be 598.6 nm. The LSPR λ_{max} shift corresponding to this surface functionalization step was a 38 nm red-shift, hereafter $+$ will signify a red-shift and $-$ a blue-shift, with respect to bare Ag nanoparticles. Next, biotin was covalently attached via amide bond formation with a two unit polyethylene glycol linker to carboxylated surface sites. The LSPR λ_{max} after biotin attachment (Fig. 5A-3) was measured to be 609.6 nm corresponding to an additional $+11$ nm shift. The LSPR nanosensor has now been prepared for exposure to the target analyte. Exposure to 100 nM streptavidin, resulted in LSPR $\lambda_{max} = 636.6$ nm (Fig. 5A-4) corresponding to an additional $+27$ nm shift.

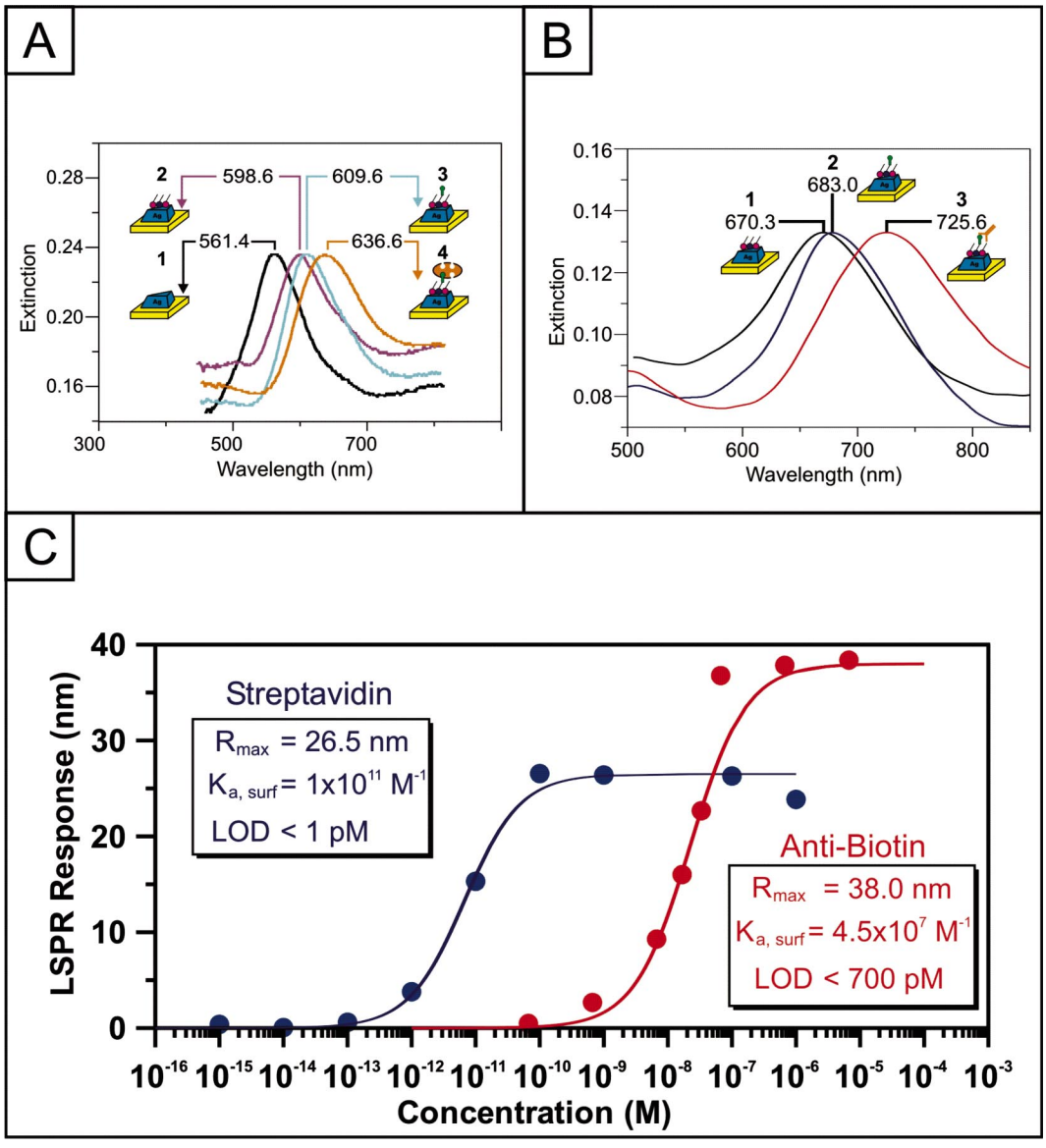

Fig. 5. (A) LSPR spectra of each step in the surface modification of NSL-derived Ag nanoparticles to form a biotinylated Ag nanobiosensor and the specific binding of streptavidin. (1) Ag nanoparticles before chemical modification, $\lambda_{max} = 561.4$ nm. (2) Ag nanoparticles after modification with 1 mM 1:3 11-MUA:1-OT, $\lambda_{max} = 598.6$ nm. (3) Ag nanoparticles after modification with 1 mM biotin, $\lambda_{max} = 609.6$ nm. (4) Ag nanoparticles after modification with 100 nM streptavidin, $\lambda_{max} = 636.6$ nm. All extinction measurements were collected in a N_2 environment. (B) Smoothed LSPR spectra for each step of the preparation of the Ag nanobiosensor, and the specific binding of anti-biotin to biotin. (1) Ag nanoparticles after modification with 1 mM 3:1 1-OT/11-MUA, $\lambda_{max} = 670.3$ nm, (2) Ag nanoparticles after modification with 1 mM biotin, $\lambda_{max} = 683.0$ nm, and (3) Ag nanoparticles after modification with 700 nM anti-biotin, $\lambda_{max} = 725.6$ nm. All spectra were collected in a N_2 environment. (C) The specific binding of streptavidin (left) and anti-biotin (right) to a biotinylated Ag nanobiosensor is shown in the response curves. All measurements were collected in a N_2 environment. The solid line is the calculated value of the nanosensor's response. Reproduced with permission from J. Am. Chem. Soc. 2002, 124, 10596–10604. Copyright 2002 Am. Chem. Soc. Reproduced with permission from J. Phys. Chem. B 2003 107, 1772–1780. Copyright 2003 Am. Chem. Soc.

It should be noted that the signal transduction mechanism in this nanosensor is a reliably measured wavelength shift rather than an intensity change as in many previously reported nanoparticle-based sensors [6,88].

ANTI-BIOTIN SENSING ON NANOPARTICLE ARRAYS USING LSPR SPECTROSCOPY

A field of particular interest is the study of the interaction between antigens and antibodies. [89] For these reasons we have chosen to focus the present LSPR review on a prototypical immunoassay involving biotin and anti-biotin, an IgG antibody. In this study, we report the use of Ag nanotriangles synthesized using NSL as a LSPR biosensor that monitors the interaction between a biotinylated surface and free anti-biotin in solution [24]. The importance of this study is that it demonstrates the feasibility of LSPR biosensing with a biological couple whose binding affinity is significantly lower ($1.9 \times 10^6 - 4.98 \times 10^8$ M^{-1}) [90,91] than in the biotin/streptavidin model.

Just as in the streptavidin assay, NSL was used to create massively parallel arrays of Ag nanotriangles on a mica substrate. A SAM of 1:3 1-MUA:1-OT was formed on the surface by incubation for 24 hr. As in the streptavidin experiments, a zero length coupling agent was then used to covalently link biotin to the carboxylate groups.

Each step of the functionalization of the samples was monitored using UV-vis spectroscopy, as shown in Fig. 5B. After a 24 hr incubation in SAM, the LSPR extinction wavelength of the Ag nanoparticles was measured to be 670.3 nm (Fig. 5B-1). Samples were then incubated for 3 hr in biotin to ensure that the amide bond between the amine and carboxyl groups had been formed. The LSPR wavelength shift due to this binding event was measured to be +12.7 nm, resulting in a LSPR extinction wavelength of 683.0 nm (Fig. 5B-2). At this stage, the nanosensor was ready to detect the specific binding of anti-biotin. Incubation in 700 nM anti-biotin for 3 hr resulted in a LSPR wavelength shift of +42.6 nm, giving a λ_{max} of 725.6 nm (Fig. 5B-3).

MONTIORING THE SPECIFIC BINDING OF STREPTAVIDIN TO BIOTIN AND ANTI-BIOTIN

The well-studied biotin/streptavidin [6,88] system with its extremely high binding affinity ($K_a \sim 10^{13}$ M^{-1}) and the antigen-antibody couple, biotin/anti-biotin ($K_a \sim 10^6 - 10^8$ M^{-1}) [24] have been chosen to illustrate the attributes of these LSPR-based nanoscale affinity biosensors. The LSPR λ_{max} shift, ΔR, vs. [analyte] response curve was measured over the concentration range 1×10^{-15} M < [streptavidin] < 1×10^{-6} M and 7×10^{-10} M < [anti-biotin] < 7×10^{-6} M (Fig. 5C) [6,24]. Each data point is an averaged resulted from the analysis of three different samples at identical concentrations. The lines are not a fit to the data. Instead, the line was computed from a response model [24]. described by

$$\Delta R = \Delta R_{\max}\left(\frac{K_{a,surf}[\text{Analyte}]}{1 + K_{a,surf}[\text{Analyte}]}\right) \qquad (3)$$

where ΔR is the nanosensor's response for a given analyte concentration, [Analyte], ΔR_{max} is the maximum sensor response for a full monolayer coverage, and $K_{a,surf}$ is the surface confined binding constant. It was found that this response could be interpreted quantitatively in terms of a model involving: (1) 1:1 binding of a ligand to a multivalent receptor with different sites but invariant affinities and (2) the assumption that only adsorbate-induced local refractive index changes were responsible for the operation of the LSPR nanosensor.

The binding curve provides three important characteristics regarding the system under study. First, the mass and dimensions of the molecules affect the magnitude of the LSPR shift response. Comparison of the data with theoretical expectations yielded a saturation response, $\Delta R_{max} = 26.5$ nm for streptavidin, a 60 kDa molecule, and 38.0 nm for anti-biotin, a 150 kDa molecule. Clearly, a larger mass density at the surface of the nanoparticle results in a larger LSPR response. Next, the surface-confined thermodynamic binding constant $K_{a,surf}$ can be calculated from the binding curve and is estimated to be 1×10^{11} M^{-1} for streptavidin and 4.5×10^7 M^{-1} for anti-biotin. These numbers are directly correlated to the third important characteristic of the system, the limit of detection (LOD). The LOD for the unoptimized nanoparticle sensor is less than 1 pM for streptavidin and 100 pM for anti-biotin. As predicted, the LOD of the nanobiosensor studied is lower for systems with higher binding affinities such as for the well-studied biotin-streptavidin couple and higher for systems with lower binding affinities as seen in the anti-biotin system.

REVERSIBILITY

In order for LSPR nanobiosensors to fulfill their mandate, they must be biocompatible and operate under physiological conditions. Some binding interactions such as poly-L-lysine to a negatively charged surface can interact reversibly, while other couples with higher surface binding affinities interact irreversibly. Ideally, a commercially viable nanobiosensor should be entirely reusable. In the case

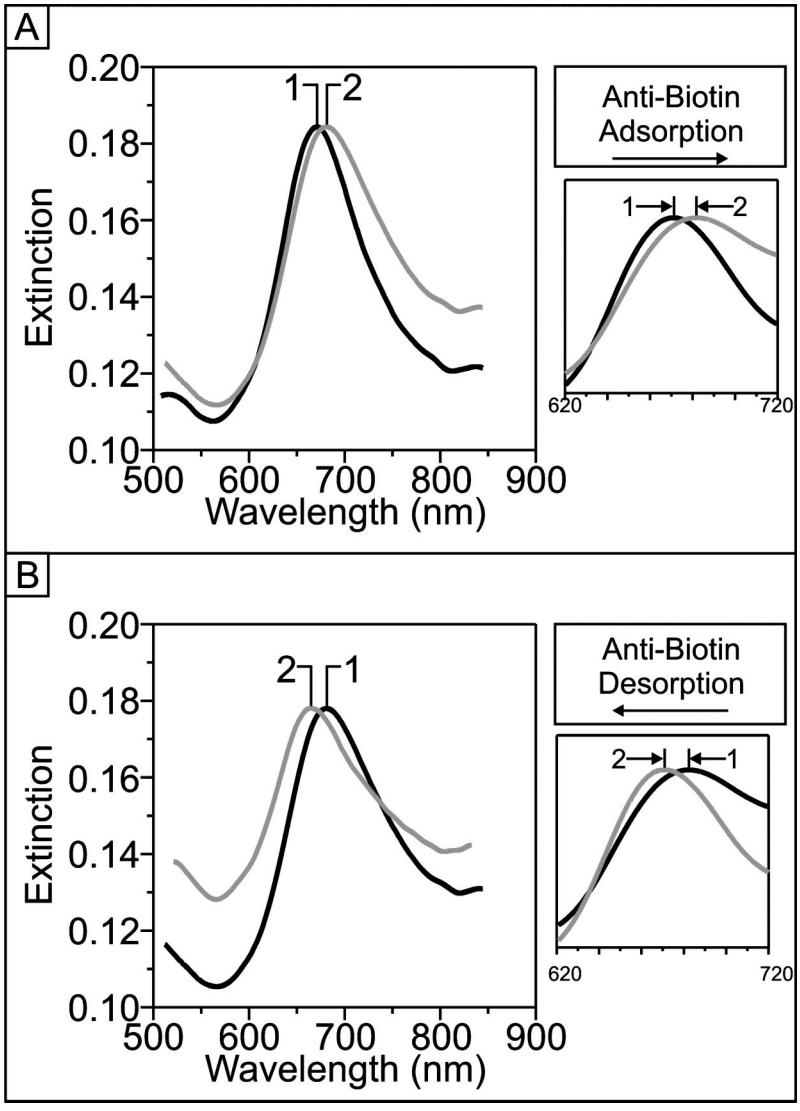

Fig. 6. An LSPR sensing experiment shows the adsorption/desorption of 20 nM anti-biotin to biotinylated Ag nanoparticles in solution. (A) Anti-biotin is adsorbed onto biotinylated nanoparticles: (1) LSPR spectrum of biotinylated Ag nanoparticles in buffer, $\lambda_{max} = 671.1$ nm, (2) LSPR spectrum of Ag nanoparticles after incubation in 20 nM anti-biotin buffer, $\lambda_{max} = 681.8$ nm. (B) Anti-biotin is desorbed onto biotinylated nanoparticles: (2) LSPR spectrum of biotinylated Ag nanoparticles after incubation in 20 nM anti-biotin in buffer, $\lambda_{max} = 681.8$ nm, (2) LSPR spectrum of Ag nanoparticles after incubation in an excess of biotin in buffer for 30, $\lambda_{max} = 670.2$ nm. Reproduced with permission from J. Phys. Chem. B 2003 107, 1772–1780. Copyright 2003 Am. Chem. Soc.

of this study, this means that the analyte that is detected must be entirely removable rendering the sensor reusable. Reusability has a large impact on cost effectiveness and the simplicity of use of biosensors.

The reversibility of the binding between anti-biotin and biotin was tested experimentally by exposing an anti-biotin functionalized sample to an excess of concentrated biotin (1 mM in 10 mM buffer) (Fig. 6) [24]. The empty binding sites on the anti-biotin molecules make the molecule susceptible to removal in these conditions. The LSPR spectra [24] of a sample before treatment with anti-biotin revealed a $\lambda_{max} = 671.1$ nm (Fig. 6A-1). After incubation in 20 nM anti-biotin for 3 hr, the LSPR extinction wavelength was $\lambda_{max} = 681.8$ nm, a shift of

+10.7 nm (Fig. 6A-2). After 30 s of exposure to the 1 mM biotin, the LSPR extinction wavelength λ_{max} blue-shifted to 670.2 nm, a shift of −11.6 nm (Fig. 6BS). Considering sensor and detector limitations, this value of λ_{max} is essentially identical to its value before treatment with anti-biotin suggesting that the analyte layer was completely removed. All measurements were made in 10 mM buffer to ensure the applicability of the results to biological sensing. To fully understand and characterize this phenomenon, real time kinetic studies of the binding and desorption of anti-biotin and the adsorption of biotin to the nanoparticle surface must be performed. The time scale for these events appears to be less than a minute, except for the coupling of the linker, which is significantly slower. Such studies would also reveal useful kinetic data about the interaction of biotin and the analyte [92–95], and could provide a supplementary tool to measure the surface binding affinity between the two.

SELECTIVITY

Although LSPR spectroscopy is a totally nonselective sensor platform, a high degree of analyte selectivity can be conferred using the specificity of surface-attached ligands and passivation of the sensor surface to nonspecfic binding. For this reason, a set of control experiments were performed to show that the (A) streptavidin and anti-biotin binding to the sensor surface containing no capture ligand (biotin), (B) pre-biotinylated streptavidin binding to a sensor surface with biotin, and (C) bovine serum albumin in large excess, simulating a clinical sample, binding to a sensor surface with biotin all produce wavelength shift responses less than that corresponding to the LOD [24].

SINGLE NANOPARTICLE SPECTROSCOPY

A method to dramatically decrease the number molecules needed to induce a sensing shift for the array sensor would be to decrease the number of nanoparticles probed in a given experiment. The ultimate limit of this technique is to perform the assay on a single nanoparticle. The extension of LSPR sensing technique to the single nanoparticle limit provides several improvements over existing array- or cluster-based techniques. First, absolute detection limits are dramatically reduced. The surface area of chemically prepared Ag nanoparticles is typically less than 20,000 nm^2, which requires that a complete monolayer of adsorbate must constitute fewer than approximately 100 zeptomole. Recently, McFarland and Van Duyne demonstrated that single Ag nanoparticles can be used to sense local refractive index changes induced via bulk solvent changes and a monolayer of alkanethiols [2]. Using dark-field microscopy, the LSPR extinction maximum response of individual Ag nanoparticles to the adsorption of less than 60,000 hexadecanethiol molecules is ∼40 nm. Additionally, kinetic responses were monitored and were found to be competitive with other real-time sensors. This suggests that the limit of detection for single nanoparticle-based LSPR sensing will be well below 1,000 molecules for small molecule adsorbates. For larger molecules such as antibodies and proteins that result a greater change in the local dielectric environment upon surface adsorption, the single molecule detection limit may be achieved. Second, the extreme sensitivity of single nanoparticle sensors dictates that only very small sample volumes (viz., attoliters) are necessary to induce a measurable response. This characteristic would eliminate the need for analyte amplification techniques (e.g., polymerase chain reaction and enzyme amplification) required by other analytical methods. Third, single nanoparticle sensing platforms are readily applicable to multiplexed detection schemes. By controlling the size, shape, and chemical modification of individual nanoparticles, multiple sensing platforms can be generated in which each unique nanoparticle can be distinguished from the others based on the spectral location of its LSPR. Several of these unique nanoparticles can then be incorporated into one device, allowing for the rapid, simultaneous detection of thousands of different chemical or biological species.

The key to exploiting single nanoparticles as sensing platforms is developing a technique to monitor the LSPR of individual nanoparticles with a reasonable signal-to-noise ratio. UV-visible absorption spectroscopy does not provide a practical means of accomplishing this task. Even under the most favorable experimental conditions, the absorbance of a single nanoparticle is very close to the shot noise-governed limit of detection. Instead, resonant Rayleigh scattering spectroscopy is the most straightforward means of characterizing the optical properties of individual metallic nanoparticles. Similar to fluorescence spectroscopy, the advantage of scattering spectroscopy lies in the fact that the scattering signal is being detected in the presence of a very low background. The instrumental approach for performing these experiments generally involves using high magnification microscopy coupled with oblique or evanescent illumination of the nanoparticles. Klar *et al.* utilized a near-field scanning optical microscope coupled to a tunable laser source to measure the scattering spectra of individual gold nanoparticles embedded in a TiO_2 film [96]. Sonnichsen *et al.* were able to measure the scattering spectra of individual EBL-fabricated nanoparticles using conventional light microscopy [97].

Their technique involved illuminating the nanoparticles with the evanescent field produced by total internal reflection of light in a glass prism. The light scattered by the nanoparticles was collected with a microscope objective and coupled into a spectrometer for analysis. Matsuo and Sasaki employed differential interference contrast microscopy to perform time-resolved laser scattering spectroscopy of single silver nanoparticles [98]. Mock *et al.* correlated conventional dark-field microscopy and TEM in order to investigate the relationship between the structure of individual metallic nanoparticles and their scattering spectra [99]. They have also used the same light microscopy techniques to study the response of the scattering spectrum to the particle's local dielectric environment by immersing the nanoparticle in oils of various refractive indexes [100].

STREPTAVIDIN SENSING WITH SINGLE NANOPARTICLES

Streptavidin sensing has also been demonstrated on single Ag nanoparticles. First, chemically synthesized Ag nanoparticles that have been dispersed on a glass coverslip is placed in a flow cell and a dark field image is collected (Fig. 7A). The slits on the spectrometer are then narrowed to monitor the scattering spectrum of a single nanoparticle. After functionalization, the LSPR of an individual nanoparticle was measured to be 508.0 nm (Fig. 7B-1). Next, 10 nM streptavidin was injected into the flow cell and the nanoparticle was allowed to incubate for 2 hr. Following this incubation and rinsing, the λ_{max} of the nanoparticle was measured at 520.7 nm (Fig. 7B-2). This $+12.7$ nm shift is estimated to arise from the detection of less than 700 streptavidin molecules.

During the course of our streptavidin experiments with single Ag nanoparticles, we became aware of a parallel research effort using Au nanoparticles and dark field microscopy [101]. The technique used by Rashke *et al.* involves functionalizing spherical Au nanoparticles with biotinylated bovine serum albumin (BSA) and monitoring the LSPR shift of a single nanoparticle during exposure to 2 μM streptavidin. The maximum LSPR shift that they observed was approximately $+1.2$ nm. This relatively small response is a consequence of four aspects of their experimental conditions: (1) all spectra were recorded while the nanoparticle was immersed in a buffer solution, (2) the binding of streptavidin inside the BSA layer causes very little change in the local dielectric environment of the nanoparticle (3) the dielectric sensitivity of Au nanoparticles is smaller than Ag nanoparticles of equivalent geometry, [102] and (4) spherical nanoparticles exhibit the lowest dielectric sensitivity ($\chi = 2$). The $+12.7$ nm response

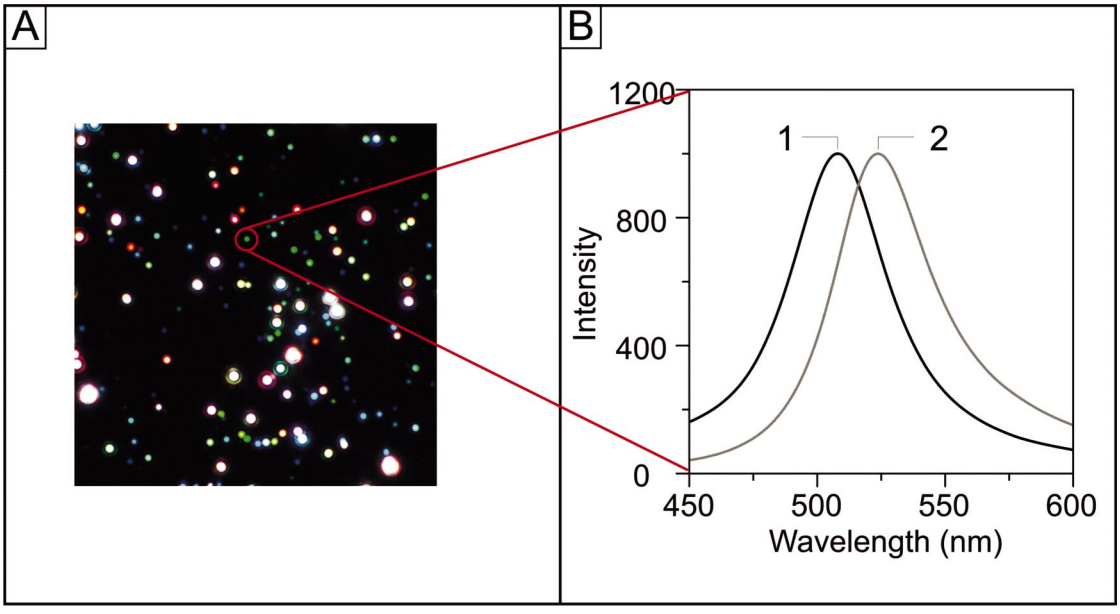

Fig. 7. (A) A dark-field optical image of a field of Ag nanoparticles. The field of view is approximately 130×170 μm. The nanoparticles were fabricated by citrate reduction of silver ions in aqueous solution and drop-coated onto a glass coverslip. (B) Individual Ag nanoparticle sensor before and after exposure to 10 nM streptavidin. All measurements were collected in a nitrogen environment. (1) Biotinylated Ag nanoparticle, $\lambda_{max} = 508.0$ nm. (2) After streptavidin incubation, $\lambda_{max} = 520.7$ nm.

demonstrated in our work is a result of the following advantages of our experimental conditions: (1) all spectra were recorded while the nanoparticle was immersed in N_2, (2) the SAM functionalization dictates that streptavidin binding causes a significant change in the local dielectric environment of the nanoparticle, (3) a Ag nanoparticle was used, and (4) the nanoparticle geometry was most likely a disk or platelet ($\chi \gg 2$) based on analysis of its LSPR spectrum and similar assignments made by Mock *et al.* [100] Because the LSPR response of nanoparticle is ultimately a function of the change in local refractive index, performing our experiment in PBS (refractive index (RI) = 1.33) as opposed to N_2 (RI = 1.00) would result in an estimated 58% decrease in response. Therefore, saturation coverage of streptavidin (RI = 1.57) would result in a +5.3 nm response even with the nanoparticle continuously immersed in PBS.

CONCLUSIONS

We have highlighted representative research accomplishments in the area of the tunable LSPR of silver and gold nanoparticles in solution and on surfaces. Specific demonstrations of using the LSPR as a signal transduction mechanism for biosensing applications in solution, on arrays of nanoparticles, and on single nanoparticles were shown. The optical properties of metallic nanostructures will find future application in the areas of dichroic filters, plasmonic waveguides, data storage, biological labels and sensors. Commercialization of nanoparticle devices relies on a better understanding of the electromagnetic interaction between nanoparticles as well as the development of techniques that will preserve nanoparticle optical activity in adverse environments.

ACKNOWLEDGMENTS

The authors gratefully acknowledge support from the Nanoscale Science and Engineering Initiative of the National Science Foundation under NSF Award Number EEC-0118025. Any opinions, findings and conclusions or recommendations expressed in this material are those of the authors and do not necessarily reflect those of the National Science Foundation. A. Haes wishes to acknowledge the American Chemical Society Division of Analytical Chemistry and Dupont for fellowship support. Support was also provided by the Air Force Office of Scientific Research MURI program (Grant F49620-02-1-0381). D. Stuart and S. Nie acknowledge NIH grant R01 GM58173.

REFERENCES

1. S. R. Nicewarner-Pena, R. Griffith Freeman, B. D. Reiss, L. He, D. J. Pena, I. D. Walton, R. Cromer, C. D. Keating, and M. J. Natan (2001). Submicrometer metallic barcodes. *Science* **294**(5540), 137–141.
2. A. D. McFarland and R. P. Van Duyne (2003). Single silver nanoparticles as real-time optical sensors with zeptomole sensitivity. *Nano Lett.* **3**, 1057–1062.
3. S. Schultz, D. R. Smith, J. J. Mock, and D. A. Schultz. (2000). Single-target molecule detection with nonbleaching multicolor optical immunolabels. *Proc. Natl. Acad. Sci. U.S.A.* **97**(3), 996–1001.
4. C. A. Mirkin, R. L. Letsinger, R. C. Mucic, and J. J. Storhoff (1996). A DNA-based method for rationally assembling nanoparticles into macroscopic materials. *Nature* **382**(6592), 607–609.
5. M. D. Malinsky, K. L. Kelly, G. C. Schatz, and R. P. Van Duyne (2001). Chain length dependence and sensing capabilities of the localized surface plasmon resonance of silver nanoparticles chemically modified with alkanethiol self-assembled monolayers *J. Am. Chem. Soc.* **123**(7), 1471–1482.
6. A. J. Haes and R. P. Van Duyne (2002). A nanoscale optical biosensor: Sensitivity and selectivity of an approach based on the localized surface plasmon resonance spectroscopy of triangular silver nanoparticles *J. Am. Chem. Soc.* **124**(35), 10596–10604.
7. A. J. Haes, S. Zou, G. C. Schatz, and R. P. Van Duyne (2004). *Nanoscale Optical Biosensor: Short Range Distance Dependence of the Localized Surface Plasmon Resonance of Noble Metal Nanoparticles*. (Submitted) *J. Phys. Chem. B. ASAP.*
8. R. G. Freeman, K. C. Grabar, K. J. Allison, R. M. Bright, J. A. Davis, A. P. Guthrie, M. B. Hommer, M. A. Jackson, P. C. Smith, D. G. Walter, and M. J. Natan (1995). Self-assembled metal colloid monolayers: An approach to SERS substrates. *Science* **267**, 1629–1632.
9. M. Kahl, E. Voges, S. Kostrewa, C. Viets, and W. Hill (1998). Periodically structured metallic substrates for SERS *Sens. Actuator B-Chem.* **51**(1–3), 285–291.
10. G. C. Schatz and R. P. Van Duyne (2002). *Electromagnetic Mechanism of Surface-Enhanced Spectroscopy*, Vol. 1, Wiley, New York.
11. C. L. Haynes and R. P. Van Duyne (2003). Plasmon-sampled surface-enhanced Raman excitation spectroscopy. *J. Phys. Chem. B* **107**, 7426–7433.
12. C. L. Haynes, A. D. McFarland, L. Zhao, R. P. Van Duyne, G. C. Schatz, L. Gunnarsson, J. Prikulis, B. Kasemo, and M. Käll (2003). Nanoparticle optics: The importance of radiative dipole coupling in two-dimensional nanoparticle arrays. *J. Phys. Chem. B* **107**, 7337–7342.
13. Y. Dirix, C. Bastiaansen, W. Caseri, and P. Smith (1999). Oriented pearl-necklace arrays of metallic nanoparticles in polymers: A new route toward polarization-dependent color filters. *Adv. Mat.* **11**, 223–227.
14. C. L. Haynes and R. P. Van Duyne (2003). Dichroic optical properties of extended nanostructures fabricated using angle-resolved nanosphere lithography. *Nano Lett.* **3**(7), 939–943.
15. S. A. Maier, M. L. Brongersma, P. G. Kik, S. Meltzer, A. A. G. Requicha, and H. A. Atwater (2001). Plasmonics-A route to nanoscale optical devices. *Adv. Mat.* **13**(19), 1501–1505.
16. S. A. Maier, P. G. Kik, H. A. Atwater, S. Meltzer, E. Harel, B. E. Koel, and A. A. G. Requicha (2003). Local detection of electromagnetic energy transport below the diffraction limit in metal nanoparticle plasmon waveguides. *Nat. Mat.* **2**, 229–232.
17. R. A. Shelby, D. R. Smith, and S. Schultz (2001). Experimental verification of a negative index of refraction. *Science* **292**(5514), 77–78.
18. R. C. Mucic, J. J. Storhoff, C. A. Mirkin, and R. L. Letsinger (1998). DNA-directed synthesis of binary nanoparticle network materials. *J. Am. Chem. Soc.* **120**, 12674–12675.

19. L. R. Hirsch, J. B. Jackson, A. Lee, N. J. Halas, and J. L. West (2003). A whole blood immunoassay using gold nanoshells *Anal. Chem.* **75**(10), 2377–2381.
20. A. J. Haes and R. P. Van Duyne (2002). A highly sensitive and selective surface-enhanced nanobiosensor. *Mat. Res. Soc. Symp. Proc.* **723**, O3.1.1–O3.1.6.
21. A. J. Haes and R. P. Van Duyne (2003). Nanosensors enable portable detectors for environmental and medical applications *Laser Focus World* **39**, 153–156.
22. A. J. Haes and R. P. Van Duyne (2003). Nanoscale optical biosensors based on localized surface plasmon resonance spectroscopy. *SPIE*, **5221**, 47–58.
23. A. J. Haes, S. Zou, G. C. Schatz, and R. P. Van Duyne (2004). A nanoscale optical biosensor: The long range distance dependence of the localized surface plasmon resonance of noble metal nanoparticles. *J. Phys. Chem. B* **108**(1), 109–116.
24. J. C. Riboh, A. J. Haes, A. D. McFarland, C. R. Yonzon, and R. P. Van Duyne (2003). A nanoscale optical biosensor: Real-time immunoassay in physiological buffer enabled by improved nanoparticle adhesion. *J. Phys. Chem. B* **107**, 1772–1780.
25. T. R. Jensen, M. D. Malinsky, C. L. Haynes, and R. P. Van Duyne (2000). Nanosphere lithography: Tunable localized surface plasmon resonance spectra of silver nanoparticles. *J. Phys. Chem. B* **104**(45), 10549–10556.
26. S. Link and M. A. El-Sayed (1999). Spectral properties and relaxation dynamics of surface plasmon electronic oscillations in gold and silver nano-dots and nano-rods. *J. Phys. Chem. B* **103**(40), 8410–8426.
27. M. A. El-Sayed (2001). Some interesting properties of metals confined in time and nanometer space of different shapes. *Acc. Chem. Res.* **34**(4), 257–264.
28. A. M. Michaels, M. Nirmal, and L. E. Brus (1999). Surface enhanced raman spectroscopy of individual rhodamine 6G molecules on large Ag Nanocrystals. *J. Am. Chem. Soc.* **121**(43), 9932–9939.
29. S. Schultz, D. R. Smith, J. J. Mock, and D. A. Schultz (2000). Single-target molecule detection with nonbleaching multicolor optical immunolabels. P.N.A.S. **97**(3), 996–1001.
30. J. Yguerabide and E. E. Yguerabide (1998). Light-scattering submicroscopic particles as highly fluorescent analogs and their use as tracer labels in clinical and biological applications-I. Theory. *Anal. Biochem.* **262**, 137–156.
31. J. Yguerabide and E. E. Yguerabide (1998). Light-scattering submicroscopic particles as highly fluorescent analogs and their use as tracer labels in clinical and biological applications-II. Experimental characterization. *Anal. Biochem.* **262**, 157–176.
32. U. Kreibig and M. Vollmer (1995) *Cluster Materials*, Vol. 25, Springer-Verlag, Heidelberg, Germany.
33. C. L. Haynes and R. P. Van Duyne (2001). Nanosphere lithography: A versatile nanofabrication tool for studies of size-dependent nanoparticle optics. *J. Phys. Chem. B* **105**(24), 5599–5611.
34. P. Mulvaney (2001). Not all that's gold does glitter. *MRS Bull.* **26**(12), 1009–1014.
35. U. Kreibig, M. Gartz, A. Hilger, and H. Hovel (1998). in M. A. Duncan (Ed.), *Advances in Metal and Semiconductor Clusters*, JAI Press, Stanford, CT pp. 345–393.
36. P. Mulvaney (1996). Surface plasmon spectroscopy of nanosized metal particles. *Langmuir* **12**(3), 788–800.
37. U. Kreibig (1997). in R. E. Hummel and P. Wissmann (Eds.), *Handbook of Optical Properties*, CRC Press, Boca Raton, FL, pp. 145–190.
38. T. R. Jensen, M. L. Duval, K. L. Kelly, A. Lazarides, G. C. Schatz, and R. P. Van Duyne (1999). Nanosphere lithography: Effect of the external dielectric medium on the surface plasmon resonance spectrum of a periodic array of silver nanoparticles. *J. Phys. Chem. B* **103**(45), 9846–9853.
39. J. C. Hulteen and R. P. Van Duyne (1995). Nanosphere lithography: A materials general fabrication process for periodic particle array surfaces. *J. Vac. Sci. Technol. A* **13**, 1553–1558.
40. J. C. Hulteen, D. A. Treichel, M. T. Smith, M. L. Duval, T. R. Jensen, and R. P. Van Duyne (1999). Nanosphere lithography: Size-tunable silver nanoparticle and surface cluster arrays. *J. Phys. Chem. B* **103**(19), 3854–3863.
41. R. Micheletto, H. Fukuda, and M. Ohtsu (1995). A simple method for the production of a two-dimensional, ordered array of small latex particles. *Langmuir* **11**, 3333–3336.
42. A. P. F. Turner (2000). Biosensors–Sense and sensitivity. *Science* **290**, 1315–1317.
43. I. M. Klotz (1997). *Ligand-Receptor Energetics: A Guide for the Perplexed*, Wiley, New York.
44. H. J. Lee, T. T. Goodrich, and R. M. Corn (2001). SPR imaging measurements of 1-D and 2-D DNA microarrays created from microfluidic channels on gold thin films. *Anal. Chem.* **73**(55), 5525–5531.
45. D. Hall (2001). Use of optical biosensors for the study of mechanistically concerted surface adsorption processes. *Anal. Biochem.* **288**(2), 109–125.
46. J. Wang, X. Cai, G. Rivas, H. Shiraishi, P. A. M. Farias, and N. Dontha (1996). DNA electrochemical biosensor for the detection of short DNA sequences related to the human immunodeficiency virus. *Anal. Chem.* **68**(15), 2629–2634.
47. H. T. Walterbeek and A. J. G. M. van der Meer (1996). A sensitive and quantitative biosensing method for the determination of γ-ray emitting radionuclides in surface water. *J. Environ. Radioact.* **33**(3), 237–254.
48. D. R. Thevenot, K. Toth, R. A. Durst, and G. S. Wilson (2001). Electrochemical biosensors: Recommended definitions and classification *Biosens. Bioelectron.* **16**(1/2), 121–131.
49. M. Mascini, I. Palchetti, and G. Marrazza (2001). DNA electrochemical biosensors. *Fresenius' J. Anal. Chem.* **369**(1), 15–22.
50. J. Horacek and P. Skladal (1997). Improved direct piezoelectric biosensors operating in liquid solution for the competitive label-free immunoassay of 2,4-dichlorophenoxyacetic acid. *Anal. Chim. Acta* **347**(1/2), 43–50.
51. R. C. Ebersole, J. A. Miller, J. R. Moran, and M. D. Ward (1990). Spontaneously formed functionally active avidin monolayers on metal surfaces: A strategy for immobilizing biological reagents and design of piezoelectric biosensors. *J. Am. Chem. Soc.* **112**(8), 3239–3241.
52. M. M. Miller, P. E. Sheehan, R. L. Edelstein, C. R. Tamanaha, L. Zhong, S. Bounnak, L. J. Whitman, and R. J. Colton (2001). A DNA array sensor utilizing magnetic microbeads and magnetoelectronic detection. *J. Magn. Magn. Mater.* **225**(1/2), 156–160.
53. Y. R. Chemla, H. L. Grossman, Y. Poon, R. McDermott, R. Stevens, M. D. Alper, and J. Clarke (2000). Ultrasensitive magnetic biosensor for homogeneous immunoassay. *Proc. Natl. Acad. Sci.* **97**, 26.
54. R. Raiteri, M. Grattarola, H.-J. Butt, and P. Skladal (2001). Micromechanical cantilever-based biosensors. *Sens. Actuators B* **B79**(2/3), 115–126.
55. B. Kasemo (1998). Biological surface science. *Curr. Opin. Solid State Mater. Sci.* **3**(5), 451–459.
56. T. Natsume, H. Nakayama, and T. Isobe (2001). BIA-MS-MS: biomolecular interaction analysis for functional proteomics. *Trends Biotechnol.* **19**(Suppl. 10), S28–S33.
57. D. L. Polla, A. G. Erdman, W. P. Robbins, D. T. Markus, J. Diaz-Diaz, R. Rizq, Y. Nam, H. T. Brickner, A. Wang, and P. Krulevitch (2000). Microdevices in medicine. *Annu. Rev. Biomed. Eng.* **2**, 551–576.
58. C. L. Baird and D. G. Myszka (2001). Current and emerging commercial optical biosensors. *J. Mol. Recognition.* **14**(5), 261–268.
59. N. Nath and A. Chilkoti (2002). A colorimetric gold nanoparticle sensor to interrogate biomolecular interactions in real time on a surface. *Anal. Chem.* **74**(3), 504–509.
60. S. Connolly, S. Cobbe, and D. Fitzmaurice (2001). Effects of ligand-receptor geometry and stoichiometry on protein-induced aggregation of biotin-modified colloidal gold. *J. Phys. Chem. B* **105**(11), 2222–2226.

61. Y. W. Cao, R. Jin, and C. A. Mirkin (2001). DNA modified core-shell Ag/Au nanoparticles. *J. Am. Chem. Soc.* **123**(32), 7961–7962.
62. P. Englebienne, A. Van Hoonacker, and M. Verhas (2001). High-throughput screening using the surface plasmon resonance effect of colloidal gold nanoparticles. *Analyst* **126**(10), 1645–1651.
63. D. Eck, C. A. Helm, N. J. Wagner, and K. A. Vaynberg (2001). Plasmon resonance measurements of the adsorption and adsorption kinetics of a biopolymer onto gold nanocolloids. *Langmuir* **17**(4), 957–960.
64. T. A. Taton, G. Lu, and C. A. Mirkin (2001). Two-color labeling of oligonucleotide arrays via size-selective scattering of nanoparticle probes. *J. Am. Chem. Soc.* **123**(21), 5164–5165.
65. J. J. Storhoff, A. A. Lazarides, R. C. Mucic, C. A. Mirkin, R. L. Letsinger, and G. C. Schatz (2000). What controls the optical properties of DNA-linked gold nanoparticle assemblies? *J. Am. Chem. Soc.* **122**(19), 4640–4650.
66. S. Connolly, S. N. Rao, and D. Fitzmaurice (2000). Characterization of protein aggregated gold nanocrystals. *J. Am. Chem. Soc.* **104**(19), 4765–4776.
67. T. Okamoto, I. Yamaguchi, and T. Kobayashi (2000). Local plasmon sensor with gold colloid monolayers deposited upon glass substrates. *Opt. Lett.* **25**(6), 372–374.
68. M. Himmelhaus and H. Takei (2000). Cap-shaped gold nanoparticles for an optical biosensor. *Sens. Actuators, B* **B63**(1/2), 24–30.
69. G. Bauer, F. Pittner, and T. Schalkhammer (1999). Metal nanocluster biosensors. *Mikrochim. Acta* **131**(1/2), 107–114.
70. H. Takei (1998). Biological sensor based on localized surface plasmon associated with surface-bound au/polystyrene composite microparticles. *Proc. SPIE-Int. Soc. Opt. Eng.* **3515**, 278–283.
71. P. Englebienne (1998). Use of colloidal gold surface plasmon resonance peak shift to infer affinity constants from the interactions between protein antigens and antibodies specific for single or multiple epitopes. *Analyst* **123**(7), 1599–1603.
72. G. Steiner, M. T. Pham, C. Kuhne, and R. Salzer (1998). Surface plasmon resonance within ion-implanted silver clusters. *Fresenius' J. Anal. Chem.* **362**(1), 9–14.
73. J. J. Storhoff, R. Elghanian, R. C. Mucic, C. A. Mirkin, and R. L. Letsinger (1998). One-pot colorimetric differentiation of polynucleotides with single base imperfections using gold nanoparticle probes. *J. Am. Chem. Soc.* **120**(9), 1959–1964.
74. R. Elghanian, J. J. Storhoff, R. C. Mucic, R. L. Letsinger, and C. A. Mirkin (1997). Selective colorimetric detection of polynucleotides based on the distance-dependent optical properties of gold nanoparticles. *Science* **227**(5329), 1078–1080.
75. G. Kalyuzhny, A. Vaskevick, G. Ashkenasy, and A. Shanzer (2000). UV/Vis spectroscopy of metalloporphyrin and metallophthalocyanine monolayers self-assembled on ultrathin gold films. *J. Phys. Chem. B* **104**(34), 8238–8244.
76. A. Hilger, N. Cuppers, M. Tenfelde, and U. Kreibig (2000). Surface and interface effects in the optical properties of silver nanoparticles. *Eur. Phys. J. D* **10**(1), 115–118.
77. G. Kalyuzhny, M. A. Schneeweiss, A. Shanzer, A. Vaskevich, and I. Rubinstein (2001). Differential plasmon spectroscopy as a tool for monitoring molecular binding to ultrathin gold films *J. Am. Chem. Soc.* **123**(12), 3177–3178.
78. M. Sanekata and I. Suzuka (2000). Physical and chemical interface effects on Mie plasmon absorption of sodium nanoclusters passivated with CH4-nCln ($n = 1$–4) molecules. *Chem. Phys. Lett.* **323**(1/2), 98–104.
79. A. Henglein and D. Meisel (1998). Spectrophotometric observations of the adsorption of organosulfur compounds on colloidal silver nanoparticles. *J. Phys. Chem. B* **102**(43), 8364–8366.
80. U. Kreibig, M. Gartz, and A. Hilger (1997). Mie resonances. Sensors for physical and chemical cluster interface properties. *Ber. Bunsen-Ges.* **101**(11), 1593–1604.
81. J. M. Singer and C. M. Plotz (1956). The latex fixation test I Application to the serologic diagnosis of rheumatoid arthritis. *Am. J. Med* **21**, 888–896.
82. T. A. Taton, C. A. Mirkin, and R. L. Letsinger (2000). Scanometric DNA array detection with nanoparticle probes. *Science* **289**(5485), 1757–1760.
83. J. J. Storhoff, R. Elghanian, C. A. Mirkin, and R. L. Letsinger (2002). Sequence-dependent stability of DNA-modified gold nanoparticles. *Langmuir* **18**(17), 6666–6670.
84. D. Roll, J. Malicka, I. Gryczynski, Z. Gryczynski, and J. R. Lakowicz (2003). Metallic colloid wavelength-ratiometric scattering sensors. *Anal. Chem.* **75**(14), 3440–3445.
85. N. M. Green (1975). Avidin. *Adv. Proten Chem.* **29**, 85–133.
86. L. S. Jung, K. E. Nelson, P. S. Stayton, and C. T. Campbell (2000). Binding and dissociation kinetics of wild-type and mutant streptavidins on mixed biotin-containing Alkylthiolate Monolayers. *Langmuir* **16**(24), 9421–9432.
87. V. H. Perez-Luna, M. J. O'Brien, K. A. Opperman, P. D. Hampton, G. P. Lopez, L. A. Klumb, and P. S. Stayton (1999). Molecular recognition between genetically engineered streptavidin and surface-bound biotin. *J. Am. Chem. Soc.* **121**(27), 6469–6478.
88. M. Wilchek and E. A. Bayer (1998). in T. Cass and F. S. Ligler (Eds.), *Avidin-Biotin Immobilization Systems*, Oxford University Press, Oxford, pp. 15–34.
89. M. Suzuki, F. Ozawa, S. Wakako, and S. Aso (2002). Miniature surface-plasmon resonance immunosensors - Rapid and repetitive procedure. *Anal. Bioanal. Chem.* **372**, 301–304.
90. N. J. Lynch, R. K. Kilpatrick, and R. G. Carbonell (1996). Aggregation of ligand-modified liposomes by specific interactions with proteins. II: Biotinylated liposomes and antibiotin antibody. *Biotechnol. Bioeng.* **50**, 169–183.
91. M. Adamczyk, P. G. Mattingly, K. Shreder, and Z. Yu (1999). Surface Plasmon Resonance (SPR) as a tool for antibody conjugate analysis. *Bioconjugate Chem.* **10**, 1032–1037.
92. P. Schuck (1997). Use of surface plasmon resonance to probe the equilibrium and dynamic aspects of interactions between biological macromolecules. *Annu. Rev. Biophys. Biomol. Struct.* **26**, 541–566.
93. L. S. Jung and C. T. Campbell (2000). Sticking probabilities in adsorption of alkanethiols from liquid ethanol solution onto gold. *J. Phys. Chem. B* **104**(47), 11168–11178.
94. L. S. Jung and C. T. Campbell (2000). Sticking probabilities in adsorption from liquid solutions: Alkylthiols on gold. *Phys. Rev. Lett.* **84**(22), 5164–5167.
95. B. L. Frey and R. M. Corn (1996). Covalent attachment and derivatization of poly(L-Lysine) monolayers on gold surfaces as characterized by polarization-modulation FT-IR spectroscopy *Anal. Chem.* **68**(18), 3187–3193.
96. T. Klar, M. Perner, S. Grosse, G. von Plessen, W. Spirkl, and J. Feldmann (1998). Surface-plasmon resonances in single metallic nanoparticles. *Phys Rev. Lett.* **80**(19), 4249–4252.
97. C. Sonnichsen, S. Geier, N. E. Hecker, G. von Plessen, J. Feldmann, H. Ditlbacher, B. Lamprecht, J. R. Krenn, F. R. Aussenegg, V. Z.-H. Chan, J. P. Spatz, and M. Moller (2000). Spectroscopy of single metallic nanoparticles using total internal reflection microscopy. *Appl. Phys. Lett.* **77**(19), 2949–2951.
98. Y. Matsuo and K. Sasaki (2001). Time-resolved Laser scattering spectroscopy of a single metallic nanoparticle. *Jpn. J. Appl. Phys.* **40**, 6143–6147.
99. J. J. Mock, S. J. Oldenburg, D. R. Smith, D. A. Schultz, and S. Schultz (2002). Composite plasmon resonant nanowires. *Nano Lett.* **2**. Web Release date: 20-Apr.
100. J. J. Mock, D. R. Smith, and S. Schultz (2003). Local refractive index dependence of plasmon resonance spectra from individual nanoparticles. *Nano Lett.* **3**(4), 485–491.
101. G. Raschke, S. Kowarik, T. Franzl, C. Sonnichsen, T. A. Klar, and J. Feldmann (2003). Biomolecular recognition based on single gold nanoparticle light scattering. *Nano Lett.* **3**(7), 935–938.
102. E. D. Palik (1985). *Handbook of Optical Constants of Solids*, Academic Press, New York.